Impact of receptor-ligand distance on adhesion cluster stability

T. Erdmann[a] and U.S. Schwarz[b]

University of Heidelberg, Im Neuenheimer Feld 293, 69120 Heidelberg, Germany

Abstract. Cells in multicellular organisms adhere to the extracellular matrix through two-dimensional clusters spanning a size range from very few to thousands of adhesion bonds. For many common receptor-ligand systems, the ligands are tethered to a surface via polymeric spacers with finite binding range, thus adhesion cluster stability crucially depends on receptor-ligand distance. We introduce a one-step master equation which incorporates the effect of cooperative binding through a finite number of polymeric ligand tethers. We also derive Fokker-Planck and mean field equations as continuum limits of the master equation. Polymers are modeled either as harmonic springs or as worm-like chains. In both cases, we find bistability between bound and unbound states for intermediate values of receptor-ligand distance and calculate the corresponding switching times. For small cluster sizes, stochastic effects destabilize the clusters at large separation, as shown by a detailed analysis of the stochastic potential resulting from the Fokker-Planck equation.

PACS. 87.15.-v Biomolecules: structure and physical properties – 82.39.-k Chemical kinetics in biological systems – 05.10.Gg Stochastic analysis methods (Fokker-Planck, Langevin, etc.)

1 Introduction

Cells adhere to the extracellular matrix or to each other through a multitude of weak interactions. The transient character of their adhesions allows cells to adapt quickly to changes in their environment. In particular, cell adhesion has to be transiently down-regulated during important physiological processes like migration or division. For tissue cells, the main receptors for cell-matrix adhesion are integrins, which are linked on the extracellular side to ligands like fibronectin and on the cytoplasmic side to the actin cytoskeleton [1]. This provides structural integrity between extracellular matrix and cytoskeleton, which is important because cell-matrix adhesion clusters usually have to operate under considerable mechanical load. The behaviour of single receptor-ligand bonds under force was first discussed by Bell [2], who suggested that bond lifetime is reduced exponentially by an applied load. This concept has been impressively confirmed and extended by dynamic force spectroscopy [3–7], which showed that binding strength can only be defined in a dynamical context. In particular, it has been shown both theoretically and experimentally that for linearly increasing load, binding strength increases linearly with the logarithm of loading rate. If loading occurs through a soft polymeric linker, binding strength is decreased compared to loading at the

same speed but through a rigid linker [8]. In practice, cell adhesion does not work with single bonds, but with clusters of bonds. It has been noted earlier that the distribution of load over the receptors in a finite-sized cluster induces non-trivial cooperativity between adhesion bonds: as one bond is disrupted, the load on the remaining bonds increases and cluster stability diminishes [2,9–11]. Likewise, as a new bond is established, the other bonds feel less force and cluster stability is enhanced.

For many common receptor-ligand systems, the ligands are tethered to a surface through polymeric spacers. This reduces the disturbance of ligand structure to preserve its specificity and allows exploration of space for receptors so that the effective affinity of surfaces covered with specific bonds is increased. For example, it has been shown recently in a macroscopic shearing experiment for streptavidin-biotin bonded beads that bonding is enhanced if ligands are tethered with polymeric spacers [12]. Thus the distance between ligands and receptors is an important determinant for specific adhesion. When cells adhere to and eventually spread on a surface, the distance between the ligand- and receptor-carrying surfaces decreases from the μm- to the nm-range on the time scale of minutes [13]. The final receptor-ligand distance for integrins is of the order of 15–20 nm, which is bridged by the polymer spacer carrying the ligand.

During recent years, the distance-dependent binding of tethered ligands has been investigated experimentally as well as theoretically. In experiments using the

---

[a] *Present address*: FOM Institute for Atomic and Molecular Physics, Kruislaan 407, 1098 SJ Amsterdam, The Netherlands.
[b] e-mail: `Ulrich.Schwarz@iwr.uni-heidelberg.de`

surface force apparatus and high-affinity streptavidin-biotin bonds [14,15], it has been shown that binding depends on rare, strongly extended conformations of the spacers and that the onset of binding is followed by a very fast increase of the fraction of bound tethers. Binding of tethered ligands to receptors has been described using a combination of Monte Carlo simulations and reaction-diffusion theory. Simulations of pearl-bead chains confined between two walls were used to determine the force-extension relation for the polymers and to derive a potential landscape for the movement of the ligands. Later reversible tethered bonds have been treated as deep but finite potential wells in the polymer potential landscape derived from simulations and used in the reaction-diffusion equations [16,17]. Moreover, the effect of changing receptor-ligand distance with a prescribed velocity has been discussed. It was concluded that kinetic effects are most important for strong binders with large affinity while thermodynamic equilibrium dominates for weak, reversible binders with small affinity. Recently, a theoretical treatment has also been given for receptor-ligand binding between curved surfaces, where different bonds are not equivalent for geometrical reasons [18].

It is important to note that these theoretical studies have been conducted in the framework of a mean-field description for a large numbers of independent, non-cooperative bonds. No theoretical treatment has been presented yet for the impact of receptor-ligand distance on the stability and dynamics of finite-sized clusters with cooperative bonds. Experimentally, it is well-known that the lateral arrangement of the integrins and therefore the integrin cluster size is regulated by cytoplasmic proteins like talin and α-actinin, which can bind both to the integrins and to the actin cytoskeleton [19]. Using image correlation microscopy, it has been shown for migrating cells that the integrins which are not yet organized in adhesions are already preclustered with an average cluster size of three to four [20]. With a measured area density of few hundreds of integrins per μm^2, this corresponds to a lateral distance well above 100 nm between the different mini-clusters. As the adhesion contacts nucleate and grow, integrins are increasingly clustered, until they approach a density of 1.000–10.000 per μm^2, corresponding to a lateral distance of 10–30 nm. The progression from very few to thousands of integrins per cluster suggests that finite size effects might be highly relevant in the stabilization of initial cell adhesion.

In this paper, we theoretically study the effect of feedback and cooperativity on the distance-dependent receptor-ligand binding dynamics in finite-sized adhesion clusters. To this end, we use a one-step master equation, which has been used before to study the adhesion cluster stability under mechanical load, both for constant force [11,21] and linearly rising force [22]. Here we extend this framework to include the effect of receptor-ligand distance. We start in Section 2 by introducing the appropriate one-step master equation. In addition, we derive two corresponding continuum descriptions, namely a Fokker-Planck equation and a deterministic differential (mean

field) equation. Our modeling framework can be used for any spatial distribution of the ligand in the direction normal to the substrate to which it is tethered. For simplicity, we start with a harmonic tether potential (*spring model*), which is the first order approximation for all polymer models at small extensions. In Section 3, we analyze the stationary states of the mean field equation and derive one-parameter bifurcation diagrams which show that the receptor-ligand dynamics of adhesion clusters leads to bistability between bound and unbound states. In Sections 5 and 6 we discuss stationary and dynamic properties of the master equation, respectively. In particular, we find that large adhesion clusters are stabilized in the bound state due to very large switching times to the unbound state. In Section 7 we combine our conceptual framework with the worm-like chain model for semiflexible polymers to study the effect of finite polymer contour length. We conclude in Section 8 by discussing some biological applications of our results. A short report on our main results regarding the spring model has been given before [23].

2 Model

2.1 Master equation and continuum limits

Figure 1 shows a schematic representation of our model for an adhesion cluster. The mechanical properties of the force transducer holding the receptors and of the polymeric tethers holding the ligands are represented by harmonic springs. We consider a situation in which N_t receptor-ligand pairs are arranged in parallel between the planar force transducer and the substrate. At a given time, each of these adhesion bonds can either be open or closed. All bonds are considered to be equivalent so that the state of the adhesion cluster is characterized by the number of closed bonds i alone. The number of open bonds is $N_t - i$. Because i ranges from $i = 0$ (completely unbound state) to $i = N_t$ (completely bound state), our model has $N_t + 1$ discrete states. Every bond changes its state (rebinds or ruptures) through thermally activated, stochastic transitions. The stochastic rates for these transitions will be specified below. Therefore, the stochastic variable i changes by discrete steps ± 1 (*one-step process*). The time dependence of the functions $\{p_i(t)\}_{i=0}^{N_t}$ representing the probability that i bonds are closed at time t are described by a one-step master equation which has the general form

$$\frac{dp_i}{dt} = r_{i+1}p_{i+1} + g_{i-1}p_{i-1} - \{r_i + g_i\}\,p_i. \qquad (1)$$

The forward rates g_i for the formation and the reverse rates r_i for the rupture of a closed bond have to be specified for all states $0 \leq i \leq N_t$. They have the general form $r_i = ik_{off}(i)$ and $g_i = (N_t - i)k_{on}(i)$. The reverse rate is the product of the number of closed bonds and the single bond off-rate $k_{off}(i)$ because the closed bonds rupture independently and at a given time any of them could be the next to break. The forward rate is the product of the
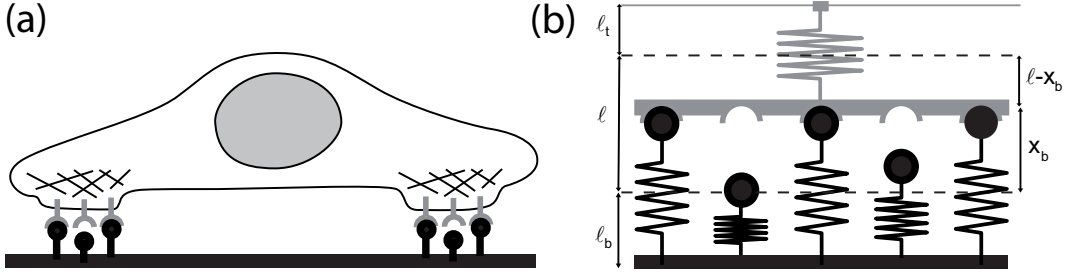
(a)

(b)

Fig. 1. (a) Cartoon of a cell adhering to a substrate through two sites of adhesion. Each adhesion corresponds to an elastic deformation in regard to the average cell-substrate distance. (b) Simple mechanical model for a site of adhesion. The cluster consists of N_t bonds (here $N_t = 5$). At a given time t, i of these bonds are closed (here 3) while $N_t - i$ (here 2) are open. The force transducer at the top (cell envelope) and the ligand tethers at the bottom are modeled as harmonic springs, with rest lengths ℓ_t and ℓ_b and spring constants k_t and k_b, respectively. The equilibrium positions of the springs (dashed lines) are separated by the receptor-ligand distance ℓ. The extensions of the bond springs and the transducer are denoted by x_b and $x_t = \ell - x_b$, respectively.

number of open bonds $(N_t - i)$ and the single bond on-rate $k_{on}(i)$ because the open bonds are independent and any one of them could be the next to bind. Both, off- and on-rate will in general depend on i. The form of the transition rates implies that the system is constrained to the interval $0 \le i \le N_t$ by two natural, reflecting boundaries at $i = 0$ and $i = N_t$, provided the single bond rates are finite at these boundaries.

If the transition rates are continuous functions of i, that is $g_i = g(i)$ and $r_i = r(i)$, it is useful to introduce a mean-field description for the average number of closed bonds, $N(t) = \langle i \rangle = \sum_{i=1}^{N_t} i p_i(t)$. The time derivative of $N(t)$ follows from the master equation (1) in terms of averages over the transition rates. Dragging the average into the argument, it can be approximated as

$$\frac{dN}{dt} = \langle g(i) \rangle - \langle r(i) \rangle \approx g(\langle i \rangle) - r(\langle i \rangle) = g(N) - r(N). \quad (2)$$

This procedure yields an ordinary differential equation for N which in the following we term the *mean field equation*. It is an exact equation for the mean number of bonds N if the transition rates are linear functions in i. Otherwise, it is only valid in the limit of large system size N_t.

To assess the role of fluctuations in the continuum limit, we derive a Fokker-Planck equation from the master equation. To achieve this, the one-step master equation (1) is written in operator form [24]

$$\frac{\partial p(i,t)}{\partial t} = \left\{ (E - 1) r(i) + (E^{-1} - 1) g(i) \right\} p(i,t) \quad (3)$$

where the operators E and E^{-1} act on the index i as

$$Ef(i) := f(i+1) \quad \text{and} \quad E^{-1} f(i) := f(i-1). \quad (4)$$

In a continuum description for i these can be expanded in a Taylor series,

$$E = 1 + \sum_{n=1}^{\infty} \frac{1}{n!} \partial_i^n \quad \text{and} \quad E^{-1} = 1 + \sum_{n=1}^{\infty} \frac{(-1)^i}{n!} \partial_i^n. \quad (5)$$

Inserting equation (5) in equation (3) leads to the Kramers-Moyal expansion [25]

$$\frac{\partial p(i,t)}{\partial t} = \left\{ -\sum_{n=0}^{\infty} \frac{\partial_i^{2n+1}}{(2n+1)!} A(i) + \sum_{n=1}^{\infty} \frac{\partial_i^{2n}}{2n!} D(i) \right\} p(i,t), \quad (6)$$

in which the Kramers-Moyal coefficients are defined by

$$A(i) = g(i) - r(i) \quad \text{and} \quad D(i) = g(i) + r(i). \quad (7)$$

The Kramers-Moyal expansion equation (6) is an exact continuum representation of the master equation. Terminating the infinite series after second order yields the Fokker-Planck equation

$$\frac{\partial p(i,t)}{\partial t} = \left\{ -\partial_i A(i) + \frac{1}{2} \partial_i^2 D(i) \right\} p(i,t) \quad (8)$$

where $A(i)$ is the drift and $D(i)$ the diffusion coefficient, which determine the short time behavior of the first and second centered moments, respectively:

$$A(i(t_0)) = \lim_{\Delta t \to 0} \frac{\langle i(t_0 + \Delta t) - i(t_0) \rangle}{\Delta t} \quad (9)$$

and

$$D(i(t_0)) = \lim_{\Delta t \to 0} \frac{\langle (i(t_0 + \Delta t) - i(t_0))^2 \rangle}{\Delta t}. \quad (10)$$

By deriving the differential equations for average and variance directly from the master equation, one can verify that the left hand sides are the derivatives dN/dt and $d\sigma^2/dt$ for the initial conditions $N(t_0) = i(t_0)$ and $\sigma^2(t_0) = 0$ at time $t = t_0$ [21,24]. The Fokker-Planck equation thus describes the average and the variance correctly. However, the centered moments of higher order are not correctly represented due to the truncation procedure.

In general, a continuous description of a one-step process through the mean field equation (2) or the Fokker-Planck equation (8) will be valid if the variation of transition rates and probability distribution is small over the

step size $\Delta i = \pm 1$. Below we will use the mean field equation for a bifurcation analysis in order to demonstrate that our system is bistable. Because the Fokker-Planck equation results from a truncated Kramers-Moyal expansion, it cannot be used to describe the full dynamics. For a bistable system it has been shown before that the diffusion approximation equation (8) leads to an error in the stationary probability distribution and an overestimation of the transition rates between the coexisting states [26]. However, this error is small for sufficiently smooth transition rates. Moreover, the extrema of the stationary distribution are correctly described by the diffusion approximation of the Fokker-Planck equation as used here. Therefore we will use it below to investigate how the stationary states are affected by thermal fluctuations which are not included in the mean field approximation. In order to describe the full stochastic dynamics, we will use the original master equation (1). Alternatively, an improved Fokker-Planck description could be used as explained in reference [26].

2.2 Transition rates

2.2.1 Reverse rate

The bond dissociation dynamics is characterized by the reverse rate $r(i)$ and strongly depends on the forces acting in the cluster. We start with the simplest possible model as suggested by the cartoon in Figure 1, that is the transducer and ligand tethers are modeled as harmonic springs with rest lengths ℓ_t and ℓ_b and spring constants k_t and k_b, respectively. Because the receptors are usually firmly attached to the actin cytoskeleton, deformation of the transducer requires a local deformation of the whole cell membrane as shown in the cartoon of Figure 1a. Therefore the stiffness k_t of the transducer is the combined stiffness of plasma membrane and cell cortex. The extensions x_b for a bound ligand and x_t for the transducer satisfy the relation $x_b + x_t = \ell$, where ℓ is the receptor-ligand distance in the completely dissociated state. In the following, we will treat the relaxed or unloaded receptor-ligand distance ℓ as a parameter which has been fixed externally, e.g. by the average cell-substrate distance or in an experiment with the surface forces apparatus. Mechanical equilibrium requires

$$iF_b = F_t = k_t x_t = k_t(\ell - x_b) = k_t\left(\ell - F_b/k_b\right) \quad (11)$$

so that

$$F_b(i) = k_b x_b(i) = \frac{k_b\ell}{1 + i(k_b/k_t)}. \quad (12)$$

The dissociation rate of a bond under force is described by the Bell model as $k_{off} = k_0 \exp\left(F_b/F_0\right)$, where k_0 is the unstressed off-rate and F_0 is the bond's internal force scale [2]. The Bell model can be rationalized in the framework of Kramers' theory for the escape over a sharp energy barrier [3]. The reverse rate $r(i)$ for the one-step master equation now follows as

$$r(i) = i k_0 \exp\left(F_b(i)/F_0\right). \quad (13)$$

When a bond ruptures, force is redistributed according to equation (12) over the smaller number of bonds so that the load on the remaining bonds increases. As a consequence, the extension of the remaining tethers increases which increases the force even further. A decrease of the number of closed bonds thus increases the off-rate for the single bonds and makes rupture of a further bond more likely. Thus the reverse rate from equation (13) describes a positive feedback mechanism for rupture which results from cooperativity in load sharing.

2.2.2 Forward rate

The bond association dynamics is characterized by the forward rate $g(i)$ and is strongly determined by the receptor-ligand distance which has to be bridged for the formation of a new bond. In the cartoon of Figure 1, the ligands are attached to springs and can move between the ligand-coated surface at the bottom and the transducer surface at the top. Hence, they move in a truncated harmonic potential, which is

$$U(x) = \frac{k_b}{2} x^2 \quad \text{if} \quad -\ell_b \le x \le x_b \quad (14)$$

and $U(x) = \infty$ otherwise. For a finite temperature T, the probability density for the ligand to be at position $x \in [-\ell_b, x_b]$ reads

$$\rho(x) = \frac{1}{Z} \exp\left(-U(x)/k_B T\right) = \frac{1}{Z} \exp\left(-k_b x^2/2 k_B T\right) \quad (15)$$

with the partition sum

$$Z = \left[\frac{\pi k_B T}{2 k_b}\right]^{\frac{1}{2}} \left\{ \mathrm{erf}\left(\left[\frac{k_b \ell_b}{2 k_B T}\right]^{\frac{1}{2}}\right) + \mathrm{erf}\left(\left[\frac{k_b x_b^2}{2 k_B T}\right]^{\frac{1}{2}}\right) \right\}. \quad (16)$$

Here $\mathrm{erf}(x) = (2/\sqrt{\pi}) \int_0^\infty \exp\left(-t^2\right) dt$ is the error function. The binding process can conceptually be divided into two steps. First, ligand and receptor have to come sufficiently close to form an encounter complex [27–30]. Second, this entangled state has to react to form the final complex. For a stationary distribution of tethers, the first step is limited by $\rho(x_b)$, the probability of the ligand to be close to the transducer surface. The second step is described by the on-rate k_{on} for the case that ligand and receptor are sufficiently close within the binding radius ℓ_{bind}. The forward rate $g(i)$ for the one-step master equation (1) thus reads

$$g(i) = k_{on}(N_t - i)\rho(x_b). \quad (17)$$

When an open bond rebinds, force is redistributed over the larger number of bonds according to equation (12) and the load on the single bonds decreases. This reduces the extension of the bound tethers and increases the density of free ligands close to the transducer. An increase of the number of closed bonds thus increases the on-rate for the single bonds and makes rebinding of a further bond

more likely. Thus the forward rate from equation (17) describes a positive feedback mechanism for binding which results from cooperativity in the formation of encounter complexes.

2.3 Adiabatic assumption

In the derivation of reverse and forward rates it was assumed that relaxation of transducer and polymer tethers to mechanical equilibrium after a change in i is fast compared to rupture and rebinding of adhesion bonds. This assumption is a prerequisite for the definition of discrete states described by the number of closed bonds alone and hence for the validity of the master equation. Experimentally it has been found for a biomembrane force probe that the damping time for the system with tethered bonds is on the order of 10^{-3} s [31], which is typically at least one order of magnitude smaller than the transition times for adhesion bonds [32]. The polymer relaxation time is determined by the Zimm time [33]. For a Flory chain, it is $\tau_Z = \eta R_F^3/k_B T$ where η is the viscosity of the surrounding fluid, R_F is the Flory radius $R_F \simeq aN^{0.6}$ with Kuhn length a and number of Kuhn segments N. The viscosity of water is on the order of $\eta \sim 10^{-3}$ Pa s. For polymers with $R_F \sim 10$ nm and for $k_B T \sim 4$ pN nm one has $\tau_Z \sim 10^{-7}$ s. This result agrees with earlier estimates for polyethylene glycol chains [14,16,18]. The very fast relaxation time scale for the polymers allows us to use a stationary density distribution for the ligands.

2.4 Dimensionless parameters

The master equation (1) together with equations (13) and (12) for the reverse rate and equations (17, 16) and (15) for the forward rate completely specifies our model. For the following, it is useful to introduce dimensionless quantities. First we introduce dimensionless time $\tau = k_0 t$. Then we non-dimensionalize all distances by writing them in units of the unstressed ligand tether length ℓ_b. The dimensionless relaxed ligand-receptor distance is denoted by $\lambda = \ell/\ell_b$. We also introduce $\kappa = k_b/k_t$, the ratio of the spring constants of bonds and transducer, and $\phi = k_b\ell_b/F_0$, the force in units of F_0 that is necessary to extend a ligand tether spring by ℓ_b, i.e. to twice its unstressed length. Then, the reverse rate reads

$$r(i) = i\exp\left(\phi\lambda/(1+\kappa i)\right) = i\exp\left(\phi\lambda(i)\right), \quad (18)$$

where $\lambda(i) = \lambda/(1+\kappa i)$ has been introduced as an abbreviation for the extension of the tethers (receptor-ligand distance with i closed bonds). Regarding the association process, we define the dimensionless on-rate $\gamma = (k_{on}/k_0)(\ell_{bind}/\ell_b)$, which is weighted with the ratio of binding radius ℓ_{bind} and unstressed tether length ℓ_b, and the inverse thermal energy $k_B T$ non-dimensionalised by the tether energy at an extension equal to their rest length, $\beta = k_b\ell_b^2/2k_B T$. Then, the forward rate reads

$$g(i) = 2\gamma(N_t - i)\left[\frac{\beta}{\pi}\right]^{\frac{1}{2}} \frac{\exp\left(-\beta\lambda^2(i)\right)}{\text{erf}\left(\beta^{\frac{1}{2}}\right) + \text{erf}\left(\beta^{\frac{1}{2}}\lambda(i)\right)}. \quad (19)$$

With the definition of these dimensionless rates, the dynamical equations, that is master equation, mean field equation and Fokker-Planck equation have the same form as in equations (1, 2) and (8), but with time derivatives in τ rather than t. Since reverse rate equation (18) and forward rate equation (19) are both non-linear in i, the mean field equation for N is only valid for large system size.

Our model now contains six dimensionless parameters. The number of receptor-ligand pairs is given by the *cluster size* N_t. The *conditional rebinding rate* γ describes the rate of binding with a flat density distribution (infinite temperature) on an interval of length ℓ_b. The *relative stiffness of the tethers*, $\kappa = k_b/k_t$, implies the two limits of $\kappa \to \infty$ (soft transducer) and $\kappa \to 0$ (stiff transducer). In the following we will use the intermediate case $\kappa = 1$. The *dimensionless force constant ϕ* measures the force needed to stretch the tethers to twice their unstressed length in units of the intrinsic force scale of the adhesion bonds. For an entropic spring, this essentially scales as the ratio of two length scales, the bond reactive compliance $k_B T/F_0$ and the rest length of the tethers. In practice it will have a rather small value and in the following we use $\phi = 0.1$. The mobility of the ligands is represented by the *inverse ligand temperature β*. In the limits of soft transducer ($\kappa \to \infty$) and very high ligand temperature ($\beta \to 0$), our model simplifies to a case which we have studied before in order to assess adhesion cluster stability under force [11,21]. In this paper, we rather focus on the role of ligand-receptor distance λ, which in combination with the different spring constants replaces the dimensionless force f used in the earlier model. In experimental setups, λ is certainly the most accessible parameter. The parameters and their definition are summarized in Table 1. There, we also give the typical range of parameters which was used for calculations and some estimates for the integrin-fibronectin system.

3 Bifurcation analysis of the mean field equation

To analyze the stationary solutions of the mean field equation, we first consider the dependence of the reverse rate $r(N)$ from equation (18) and the forward rate $g(N)$ from equation (19) on the number of closed bonds N and on the model parameters. Stationary solutions are the fixed points of equation (2) and correspond to intersections of $r(N)$ and $g(N)$, because then the time derivative $dN/d\tau = g(N) - r(N)$ vanishes. Figure 2a plots $r(N)$ and $g(N)$ as function of N for different values of the relaxed receptor-ligand distance λ. The single bond off-rate, $k_{off}(N) = \exp\left(\phi\lambda/(1+\kappa N)\right)$, is finite at $N = 0$, thus $r(0) = 0$. With increasing N, the reverse rate $r(N)$ increases almost linearly, although the single bond off-rate is a monotonous decreasing function of N. The weak influence of the exponential off-rate $k_{off}(N)$ is mainly due to the small force constant $\phi = 0.1$: the entropic tether force does not suffice to accelerate bond rupture appreciably. For larger ϕ the reverse rate increases quickly from

Table 1. The six parameters of the model: definitions, typical values used in the calculations, estimates for the integrin-fibronectin system and meaning.

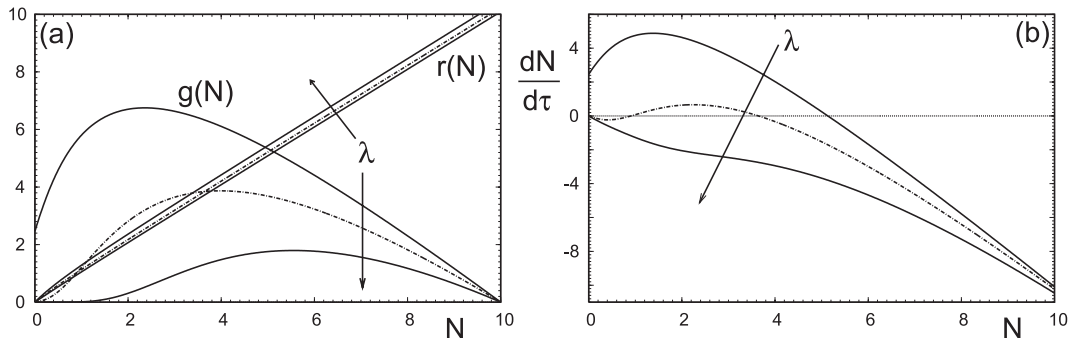| Definition	Typical	Integrins	Meaning
$\beta := k_b \ell_b^2 / 2 k_B T$	$0.1\ldots10$	7	inverse ligand temperature in units of tether energy
$\lambda := \ell / \ell_b$	$0.1\ldots10$	0.75	receptor-ligand distance
N_t	$10\ldots25$	10	cluster size
$\phi := k_b \ell_b / F_0$	0.1	0.27	tether force in units of internal force scale of bonds
$\kappa := k_b / k_t$	1	0.9	ratio of tether and transducer stiffness
$\gamma := \hat{\gamma}(\ell_{bind}/\ell_b)$	1	1	conditional single bond on-rate

Fig. 2. (a) Reverse and forward rate $r(N)$ and $g(N)$ and (b) the time derivative $dN/d\tau = g(N) - r(N)$ as a function of the number of closed bonds N for $N_t = 10$ and $\beta = 1$. The receptor-ligand distance is $\lambda = 1, 2.5$ and 5. The other parameters are $\gamma = 1$, $\kappa = 1$ and $\phi = 0.1$.

$r(0) = 0$ and can have a local maximum and minimum at small N. For large N the linear term dominates in any case. Alternatively, non-monotonous behavior could be induced by a large κ, that is for a soft transducer. The forward rate $g(N)$ vanishes for $N = N_t$, goes through a maximum at intermediate N and then decreases. At $N = 0$ the forward rates is always positive and approaches zero only in the limit of infinite β or λ. At intermediate values for λ, there are three intersections of $g(N)$ and $r(N)$. Figure 2b plots $dN/d\tau$ as function of N for the same set of parameters as in Figure 2a. It is positive at $N = 0$, because $r(0) = 0$ and $g(0) > 0$. At intermediate N and small λ, the time derivative has a maximum which reflects the maximum of $g(N)$ before it becomes negative at large N where the reverse rate dominates. The fixed point at large N is stable and represents the bound state of the adhesion cluster containing a large number of closed bonds. For intermediate λ there are three fixed points, including two stable fixed points at large N (bound state) and $N \approx 0$ (unbound state). The two stable fixed points are separated by an unstable one. At large λ there is only one stable, unbound state which approaches $N = 0$ in the limit of large λ.

Figure 3 summarizes the behavior of the fixed points in the form of two one-parameter bifurcation diagrams which show the fixed points as function of λ and β, respectively. At small separation, a single stable fixed point exists at large N. Here, the adhesion cluster is bound because the force on the bonds is small and the density of free ligands close to the receptor is large, therefore rupture events are rare and can be balanced by rebinding.

With increasing λ, the force on the bonds increases and the number of closed bonds in the bound state decreases. At large λ, there is a single stable fixed point at $N \approx 0$. Here, the adhesion cluster is unbound because forces are large and ligand density at the receptors is small so that rupture events occur frequently and cannot be balanced by rebinding. The transition from bound to unbound proceeds via two saddle-node bifurcations. At small λ, the stable unbound fixed point appears together with an unstable fixed point separating the stable ones. The unstable fixed point merges with the bound stable fixed point at larger λ. In the window of bistability between the two bifurcations, two stable fixed points coexist. The position of this window moves to smaller λ with increasing β. The bifurcation behavior as function of the inverse ligand temperature β is qualitatively similar although the position of the stable bound state initially increases with β because the forward rate initially increases. With decreasing λ, the position of the bistable range shifts to larger β while its width increases strongly.

In Figure 4 we construct a stability diagram which identifies the region of bistability as a function of λ and β. The positions of the bifurcation delineating the bistable region were determined numerically. For large β the width of the interval in λ stays almost constant while the position decreases slowly which explains the very large bistable range in β at small λ. In general, λ and β are inversely related. For the lower bifurcation one can use the approximate criterion that the slope of $dN/d\tau$ with respect to N has to become negative. Neglecting $r'(N)$, one is left with the condition $dg(N)/dN = 0$ at $N = 0$. For large $\beta \gg 1$
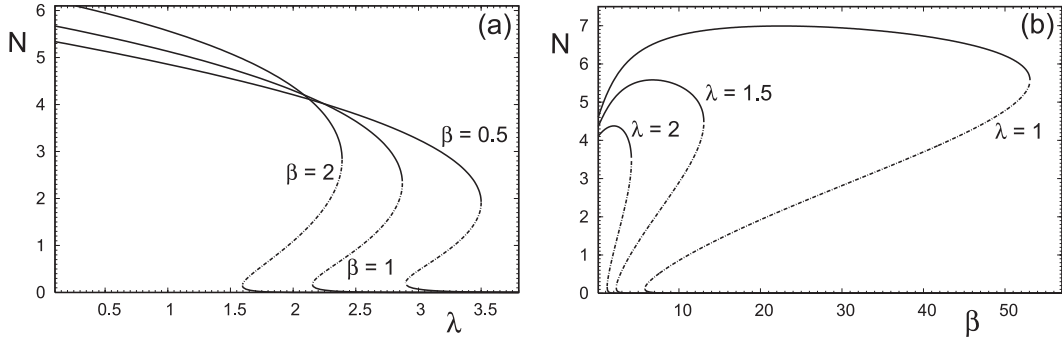
Fig. 3. One-parameter bifurcation diagrams showing the fixed points of the mean field equation for the cluster size $N_t = 10$ as function of (a) λ for $\beta = 0.5, 1$ and 2 and (b) β for $\lambda = 1, 1.5$ and 2. The stable stationary states are the solid lines, the unstable fixed points are dash-dotted. The other parameters are $\gamma = 1$, $\kappa = 1$ and $\phi = 0.1$.
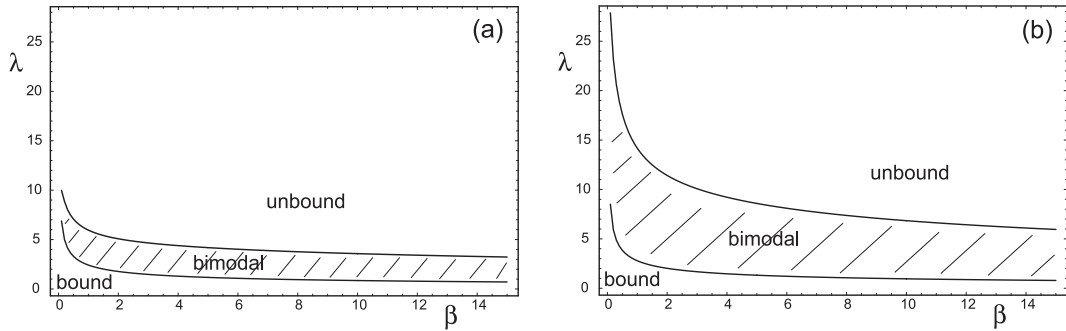

Fig. 4. Stability diagram for adhesion clusters: solid lines are numerically determined positions of the lower and upper bifurcations as function of β and λ. The shaded area between the curves is the region of bistability, above this region there is a single, unbound state while below it a single stable bound cluster exists. The curves are derived for the cluster size $N_t = 10$, $\kappa = 1$, $\phi = 0.1$ and (a) $\gamma = 1$ and (b) $\gamma = 5$.

one finds $\lambda^2 \simeq 1/(2\beta\kappa)$. For $\beta \ll 1$ and for sufficiently large λ, on the other hand, one finds $\beta \simeq \ln(\kappa N_t)/\lambda^2$. Thus in both limits, β and λ are related by an inverse square root. At small β, the width of the bistable range decreases as the two curves eventually converge and bistability vanishes. The stability diagram can be regarded as the projection of the cusp-like surface of the fixed points on the (λ, β) plane. For large clusters and also for larger on-rates γ, the curves will meet at negative β and bistability persist for positive β.

In the framework of biochemical control of biological systems, bistability is commonly associated with an underlying positive feedback mechanism [34]. In our case, bistability can arise from two positive feedback mechanisms as described above. First, there is positive feedback for bond rupture: as one bond breaks, the force on the remaining bonds increases, thus increasing their dissociation rate. Second, there is positive feedback for binding: as one ligand binds a receptor, the receptor-ligand distance is decreased and the binding rate for the other ligands is increased. In general, we verified that in our model, both mechanisms can lead to bistability. However, for the parameter range chosen here it is only the positive feedback of binding which is responsible for the observed bistability. As shown in Figure 2, the reverse rate $r(N)$ increases almost linearly for the set of parameters chosen. The forward rate $g(N)$, on the other hand, is non-monotonous.

Thus for the parameter range chosen here, the positive feedback underlying bistability is mostly due to the forward rate $g(N)$.

4 Bifurcation analysis with a stochastic potential

4.1 Stationary solution of the Fokker-Planck equation

The Fokker-Planck equation (8) has the stationary solution

$$P^s(i) = \frac{C}{D(i)} \exp\left(2 \int_0^i \frac{A(i')}{D(i')} di'\right), \qquad (20)$$

where C is a normalization constant. The integrand in the exponent exists and the expression is integrable because the Fokker-Planck coefficients are finite and defined on a compact interval. In the absence of sources and sinks the flux

$$J^s(i) = A(i)P^s(i) - \frac{1}{2}\left\{D'(i)P^s(i) + D(i)P^s(i)'\right\} \quad (21)$$

has to vanish. The derivative of $P^s(i)$ with respect to i is

$$P^s(i)' = \frac{2A(i) - D'(i)}{D(i)} P^s(i), \qquad (22)$$

so that indeed

$$J^s(i) = \left\{ A(i) - \frac{1}{2} \left\{ D'(i) + 2A(i) - D'(i) \right\} \right\} P^s(i) = 0. \tag{23}$$

In particular, the flux through the boundaries vanishes, as required for reflecting boundaries.

4.2 Stochastic potential

The stationary probability distribution equation (20) can be used to define an energy landscape $E(i)$ by

$$E(i) = -\log P^s(i). \tag{24}$$

The extrema of this potential are determined by the condition

$$\frac{dE(i)}{di} = -\frac{1}{P^s(i)} \frac{dP^s(i)}{di} = 0 \quad \Leftrightarrow \quad \frac{dP^s(i)}{di} = 0. \tag{25}$$

With equation (22) for the first derivative of the distribution, the position of the extrema of the stochastic potential $E(i)$ are thus determined by

$$A(i) - \frac{1}{2} D'(i) = 0. \tag{26}$$

These extrema have a similar physical meaning as the fixed points of the mean field equation, but they are more rigorous in including thermal fluctuations. In the framework of the stochastic potential, bistability requires a bimodal potential landscape in which two minima of the stochastic potential coexist. The coexisting minima (maxima of the probability distribution) are separated by a potential barrier (minimum of the probability distribution). The separated peaks of the probability distribution in these minima are commonly referred to as *macrostates* of the stochastic system because they are possible realizations of a macroscopic, deterministic system. One can regard the extrema as the fixed points of the dynamical system

$$\frac{di}{dt} = A(i) - \frac{1}{2} D'(i) = g(i) - r(i) - \frac{1}{2}(g'(i) + r'(i)). \tag{27}$$

This is the mean field equation corrected for the effects of non-homogeneous mobility. Equation (27) allows to determine extrema in the same way as the fixed points of the mean field equation in the previous section. For a constant diffusion coefficient the fixed points are identical to the extrema of the stochastic potential. Non-homogeneous diffusion terms change the position of fixed point and can even destroy fixed points or create new ones (*noise-induced transitions*) [35].

4.3 Bifurcation analysis

Using the stochastic dynamic system, the topology of the stochastic potential can be analyzed just as the mean field equation by deriving bifurcation diagrams showing the positions of the macrostates (the extrema of the potential) as function of the model parameters. The extrema are determined as stable and unstable fixed points of equation (27). Figure 5 shows these stochastic bifurcation diagrams as function of receptor-ligand distance λ in comparison to those from the mean field equation. For sufficiently small λ, the upper stable fixed point of the deterministic equation agrees well with a bound macrostate at large N in the stochastic potential. The saddle-node bifurcation in which the bound macrostate vanishes occurs at much smaller separation λ than in the deterministic picture, thus fluctuations destabilize the adhesion cluster. The minimum of the stochastic potential lies above the unstable deterministic fixed point and becomes negative at small λ. For positive i, the stochastic potential has no second minimum, but it has a boundary minimum at $i = 0$. This second macrostate corresponds to the unbound fixed point of the mean field equation. For larger clusters, the agreement between the fixed points of the stochastic potential and the mean field equation improves. In the limit of very large clusters, the two solution approach each other as shown in Figure 6 for $N_t = 100$ and 250. In this case, the unbound state is practically indistinguishable from $i = 0$.

5 Stationary solutions of the master equation

For a one-step master equation on a finite range without sources or sinks, stationarity $\dot{p}_i(\infty) = 0$ implies detailed balance, that is $r(i)p_i(\infty) = g(i-1)p_{i-1}(\infty)$. Iterating this relation results in the stationary probability distribution

$$\frac{p_i(\infty)}{p_0(\infty)} = \frac{g(0)}{r(i)} \prod_{j=1}^{i-1} \frac{g(j)}{r(j)} \quad \text{for } 0 < i \leq N_t. \tag{28}$$

The normalization constant is the stationary state probability for the completely dissociated state $i = 0$,

$$p_0(\infty) = \left(1 + \sum_{i=1}^{N_t} \frac{g(0)}{r(i)} \prod_{j=1}^{i-1} \frac{g(j)}{r(j)} \right)^{-1}. \tag{29}$$

Figure 7 shows a density plot of the stationary distribution $\{p_i(\infty)\}_{i=0}^{N_t}$ as function of relaxed receptor-ligand distance λ for cluster sizes $N_t = 10$ and $N_t = 25$. For small λ, there is a single peak at a finite number of closed bonds which is broadened by fluctuations. This corresponds to the bound state of adhesion clusters. For large λ, there is a single maximum at the completely dissociated state $i = 0$, which is the unbound state. In an intermediate range of λ, the stationary distribution has two maxima and bound and unbound adhesion clusters coexist. Thus the full stochastic model indeed shows bistability as suggested by the bifurcation analysis of the mean field equations. For the smaller cluster size $N_t = 10$, fluctuations are large and the transition from bound to unbound appears rather smooth. For larger systems, the transition becomes
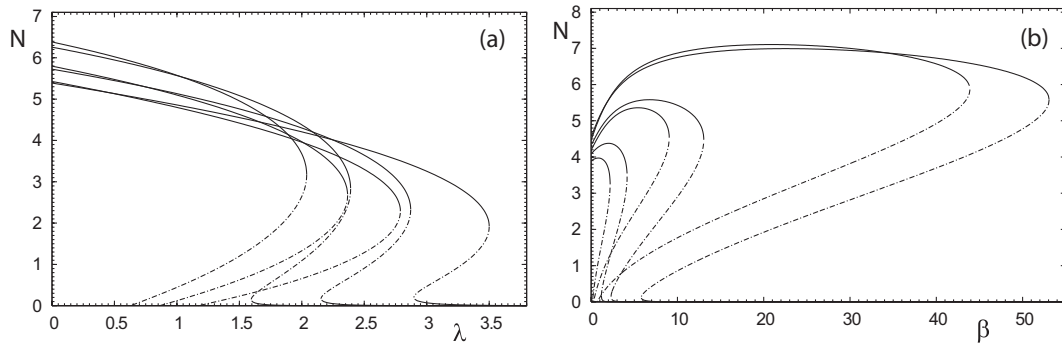
Fig. 5. Comparison of the extrema of the stochastic potential with the deterministic fixed points as function of (a) λ with $\beta = 0.5$, 1 and 2 and (b) β with $\lambda = 1$, 1.5 and 2 for the cluster size $N_t = 10$. For small parameters λ and β, stochastic and deterministic results agree well for the stable fixpoints at large N, but differ strongly in the transition regions.
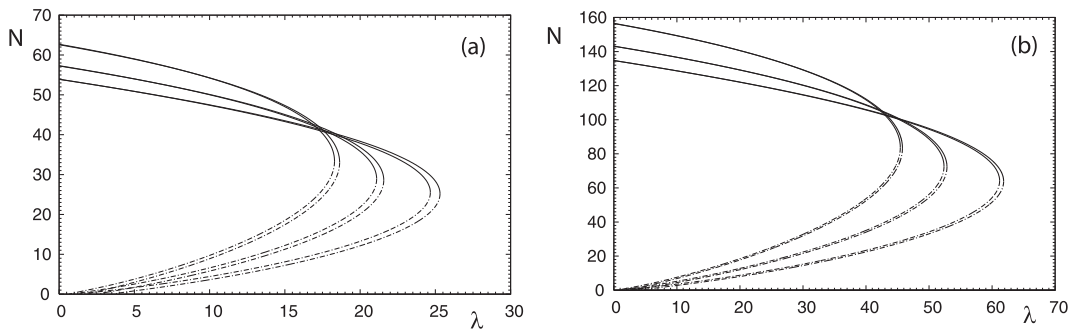

Fig. 6. Extrema of the stochastic potential as function of λ compared with the deterministic fixed points for the same parameters as in Figure 5, but for cluster sizes (a) $N_t = 100$ and (b) $N_t = 250$. For these large system sizes, stochastic and deterministic results agree well over the full range of parameters.

sharper and discontinuous. This discontinuity is demonstrated by the average number of closed bonds in the adhesion cluster which shows a steep decrease as the occupancy switches from bound to unbound. For a bimodal distribution with two distinct macrostates, average numbers of closed bonds can be defined in the two peaks separately. We use the probability functions $\{p_i(\infty)\}_{i=3}^{N_t}$ for the upper and $\{p_i(\infty)\}_{i=0}^{1}$ for the lower peak with proper normalization to calculate the average number of closed bonds in the two macrostates. Figure 7 shows that these averages vary slightly with λ and the steep decrease of the full average is mostly due to the change in occupancy probability than in the position of the peaks. Figure 7 also shows the bifurcation result from the mean field equation. For the larger system $N_t = 25$, the position of the maxima are in good agreement with the fixed points and the onset of bistability at small λ agrees well with the first bifurcation. For the smaller system $N_t = 10$, the agreement between fixed points and maxima is still good, but the onset of bimodality is overestimated by the lower bifurcation. Here, the stochastic potential yields a much better estimate for the locations of the bifurcation (not shown). For growing cluster size, the range of parameters in which the coexisting macrostates are occupied to a similar degree shrinks, although the range of bistability as revealed by the de-

terministic equation or the stochastic potential grows. In analogy to first order phase transitions, the discontinuous transition from bound to unbound will occur at a sharp parameter value in the limit of infinite clusters.

Biological systems are usually of finite size and time dependent processes are often important. Whether coexisting states and transitions between them can be observed depends on the relative occupancy of the coexisting states and on the time scale for transitions between the states. The bare presence of bistability identified in the deterministic equation is irrelevant if the time scale for the transitions is larger than the typical observation times. The time scale for transitions will also be important if parameters are time dependent. If the change of parameters is faster than the time scale for equilibration of the probability distribution, metastable states will be populated and hysteresis in the transition parameters will be observed. In the following section, we therefore analyze dynamic properties of the master equation.

6 Dynamic properties of the master equation

The stationary probability distribution equation (28) arises by averaging over many individual trajectories or over a single trajectory for a long time. Figure 8 shows
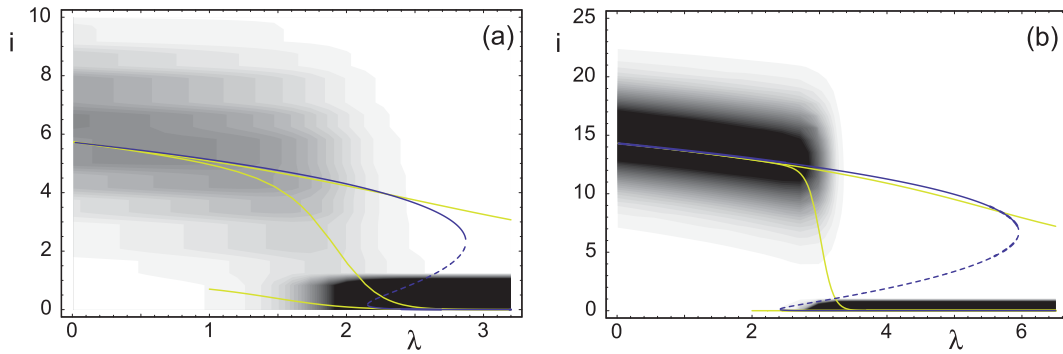
Fig. 7. Density plot of the stationary probability distribution of the master equation $\{p_i(\infty)\}_{i=0}^{\infty}$ as function of separation λ for cluster sizes (a) $N_t = 10$ and (b) $N_t = 25$. The other parameters are $\beta = 1.0$, $\gamma = 1$, $\kappa = 1$ and $\phi = 0.1$. Dark regions indicate high probability. The curves are the average number of closed bonds in the bound and unbound macrostates, in the full distribution and as predicted from the mean field equation, respectively.
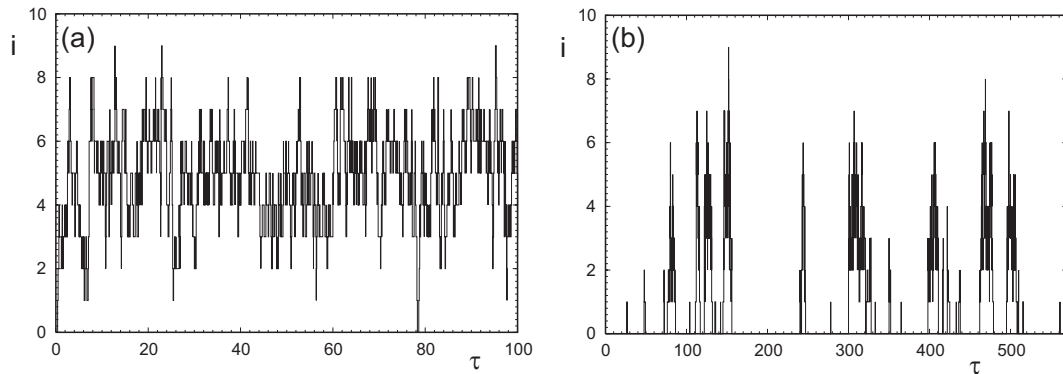

Fig. 8. Single adhesion cluster trajectories for the cluster size $N_t = 10$ at $\beta = 0.5$ at two different values of (a) $\lambda = 1$ and (b) $\lambda = 3$ generated with the Gillespie algorithm. Averaging over time or over many trajectories gives the stationary probability distribution.

two sample trajectories for $N_t = 10$ bonds and $\beta = 0.5$ at $\lambda = 1$ and $\lambda = 3$, respectively. The stochastic trajectories are generated with the Gillespie algorithm for exact stochastic simulations [36,37] and show how the number of closed bonds i changes over time. For $\lambda = 1$, the stationary distribution is unimodal and has a single peak around the bound state. Due to the small cluster size, the number of closed bonds fluctuates strongly around the average; occasionally it reaches the completely dissociated state, but rebinding takes place immediately. This leads to a single, broad peak as in Figure 7 at small λ. For $\lambda = 3$ the stationary distribution is bimodal. The sample trajectory alternates between bound and unbound state. As long as the time spent in the respective states is large enough, the time taken for the actual transition is negligible. When bound, the trajectory fluctuates around an average as in (a). An encounter of the completely dissociated state, however, is usually followed by a longer time with no or few bonds. Single closed bonds are formed occasionally, but this rarely leads to the formation of a large number of closed bonds. Increasing the receptor-ligand distance further increases the time spent in the unbound state relative to that in the bound state. This means that the

occupancy probability of the bound state is reduced. The trajectories alternating between the states with very short transition times yield the bimodal stationary distribution. The probability to find the system in one of the states is proportional to the time spent in that state before a transition. For very large λ with unimodal distribution, binding of trajectories does not take place with appreciable frequency.

The dynamic properties of the stochastic model can be characterized by the mean first passage time $T_{m,n}$ between two states m and n, that is, the time it takes on average to reach n for the first time from m. To elucidate the relevance of the fixed points in the stochastic system, the transition times from the unbound state $m = 0$ to the bound state $n \simeq N_t/2$ and vice versa are of particular interest. The value $N_t/2$ can be used because in this context it is only relevant that the bound state is above the transition barrier between the two macrostates; the dynamics within the respective basins of attraction are much faster than the dynamics across the barrier. For a one-step master equation like equation (1), the mean first passage time from the initial state m to the final state n satisfies the
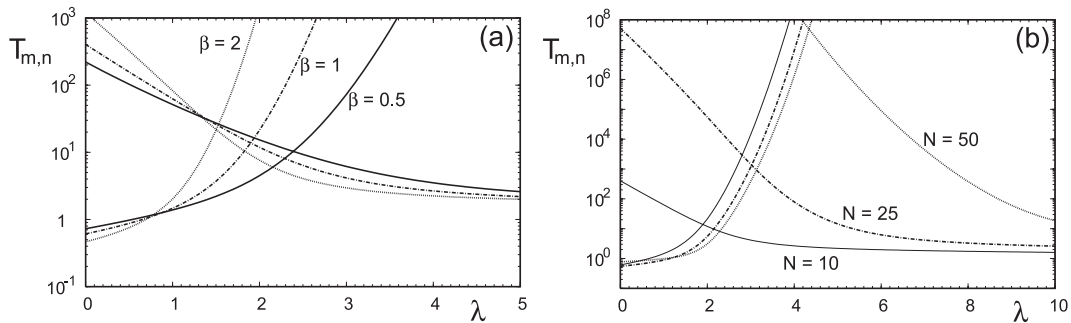
Fig. 9. Mean first passage times $T_{m,n}$ from equations (31) and (32) for transitions between unbound state $m = 0$ and unbound state $n = N_t/2$ as function of λ for (a) $N_t = 10$ and $\beta = 0.5, 1$ and 2 and (b) for $\beta = 1$ with $N_t = 10, 25$ and 50. The other parameters are $\gamma = 1$, $\kappa = 1$ and $\phi = 0.1$.

recursion relation [24]

$$g(n)\left\{T_{m+1,n} - T_{n,m}\right\} + r(m)\left\{T_{m-1,n} - T_{m,n}\right\} = -1 \tag{30}$$

with the boundary condition $T_{m,m} = 0$. For a transition from a state m to $n > m$, that is for an increase of the number of closed bonds, one has

$$T_{m,n} = \sum_{i=m}^{n-1}\left\{\frac{1}{g(i)} + \sum_{j=0}^{i-1}\frac{1}{g(j)}\prod_{k=j+1}^{i}\frac{r(k)}{g(k)}\right\}. \tag{31}$$

For the reverse transition from a state m to $n < m$, where the number of closed bonds decreases, one has

$$T_{m,n} = \sum_{i=n+1}^{m}\left\{\frac{1}{r(i)} + \sum_{j=i+1}^{N_t}\frac{1}{r(j)}\prod_{k=i}^{j-1}\frac{g(k)}{r(k)}\right\}. \tag{32}$$

The first term in curly brackets in equations (31) and (32) is the mean first passage time for a trajectory exclusively with binding or rupture, respectively. The second term with the product over the ratio of rebinding and rupture rates describes the increase of the mean first passage time through backward reactions, that is rupture if $m < n$ and rebinding if $m > n$.

Figure 9 plots the mean first passage times $T_{m,n}$ from equations (31) and (32) for transitions from the unbound state $m = 0$ to the bound state $n = N_t/2$ (binding time) and from the bound state to the unbound (unbinding time). For parameter values for which only a single stable macrostate exists, the transition time into this state is very small and on the order of magnitude of transitions between neighboring states. The time for transitions in the reverse direction becomes extremely large for large clusters. The range of bistability is characterized by binding and unbinding times which are both larger than the single step transition times. Because barrier crossing itself is a fast process, the ratio of binding to unbinding time equals the ratio of occupancy of the two macrostates in the range of bistability. The point where the transition times are equal thus defines a stochastic transition point at which both states are equally occupied. The plots of the transition times as function of λ for different β at $N_t = 10$ in Figure 9a show that this transition point shifts to larger

λ with decreasing β, because with increasing temperature (ligand mobility), larger separations can be bridged by the ligand tethers. Figure 9b plots the transition times for $\beta = 1$ at different N_t. This shows that the stochastic transition point shifts to larger separation values with growing cluster size. At the same time the corresponding switching times grow super-exponentially fast. This implies that for a given separation and growing cluster size, the bound macrostate will effectively become the only stable state; frequent switching between bound and unbound states can thus only occur for small clusters. It is important to note that these important conclusions can only be drawn by considering the full stochastic dynamics.

Stochasticity of binding and strong dependence of the mean first passage time on λ has to be considered in measurements of the binding ranges of tethered ligands. If the receptor-ligand distance is reduced step by step and the transducer is held at a constant distance during a short period of time τ_s, binding will typically be observed at a distance where the mean first passage time from unbound to bound $T(\lambda)$ is comparable to τ_s. In general, binding is always possible for all distances smaller than the contour length of the tethers. The actual binding distance is a stochastic variable. If transitions proceed with the constant rate $1/T(\lambda)$, the probability to observe binding after the nth step at a distance λ_n is

$$p = \left(1 - \exp\left(-\tau_s/T(\lambda_n)\right)\right)\prod_{i=1}^{n-1}\exp\left(-\tau_s/T(\lambda_i)\right). \tag{33}$$

With the strong dependence of the binding time on λ as shown in Figure 9 this distribution will be have a sharp peak when $T(\lambda_n) \leq \tau_s \leq T(\lambda_{i<n})$. The probability to bind at any distance below a given λ_n is then close to a step function as observed experimentally and theoretically [15,16].

7 Extension to worm-like chain model

Unlike in the simple harmonic spring model, real polymers are not infinitely extensible, but are characterized by a finite contour length. A commonly used model for real polymers is the so-called worm-like chain or Kratky-Porod

model [33]. It has been used before to model semi-flexible biopolymers like DNA, F-actin or titin [38]. A worm-like chain is characterized by the contour length L and the persistence length L_p which describes the bending stiffness of the filament. The worm-like chain model can also be extended to include elasticity of the polymer backbone which allows stretching beyond the contour length [39]. The forces needed to stretch the polymer monomers are much larger than the typical thermal forces and will not be considered in the following.

7.1 Force extension relation and rupture rate

For a worm-like chain, the force F_{wlc} which induces an average extension x of the worm-like chain polymer can be approximated by the interpolation formula [38]

$$F_{wlc}(x) = \frac{k_B T}{L_p} \left\{ \frac{1}{4(1 - (x/L))^2} + \frac{x}{L} - \frac{1}{4} \right\}. \quad (34)$$

With the first term in curly brackets the force diverges as x approaches the contour length L. The second term describes harmonic behavior at small extensions with a force constant $3k_B T/2LL_p$. The third, constant term guarantees that the force vanishes at vanishing extension. We express equation (34) in non-dimensional units by writing extension in units of the contour length, $\xi = x/L$, and force in units of the intrinsic force scale F_0 of adhesion bonds, $f_{wlc} = F_{wlc}/F_0$. The force extension relation equation (34) then reads

$$f_{wlc}(\xi) = \phi_{wlc} \left\{ \frac{1}{4(1 - \xi)^2} + \xi - \frac{1}{4} \right\} \quad (35)$$

where the ratio $\phi_{wlc} = k_B T/(F_0 L_p)$ is defined in analogy to ϕ. For small extension, $\xi \ll 1$, the constant of proportionality between ξ and f_{wlc} is $3\phi/2$.

The extension $\xi_b(i)$ of bound tethers is determined by mechanical equilibrium between tethers and transducer. In non-dimensional units this reads

$$\frac{2i\kappa_{wlc}}{3} \left\{ \frac{1}{4(1 - \xi_b(i))^2} + \xi_b(i) - \frac{1}{4} \right\} = \lambda_{wlc} - \xi_b(i) \quad (36)$$

which has to be solved for $\xi_b(i)$. The parameter $\lambda_{wlc} = \ell/L$ is the non-dimensional relaxed receptor-ligand distance and $\kappa_{wlc} = (3k_B T/2LL_p)/k_t$ measures the ratio of the harmonic force constant of the polymer and the force constant of the transducer. The two parameters are analogous to λ and κ for the spring model. Solving equation (36) for $\xi_b(i)$ yields tether extension and force $f_{wlc}(\xi_b(i))$ as function of the number of bound tethers alone. This result has to be inserted into Bell's expression $k_{off} = e^{f_{wlc}(i)}$, leading to the reverse rate of the adhesion cluster

$$r(i) = i e^{f_{wlc}(i)} \quad (37)$$

which has to be used in the one-step master equation (1) and the mean field equation (2). As a polynomial of third order, equation (36) can be easily solved for $\xi_b(i)$.

7.2 Rebinding rate

The energy needed to stretch a worm-like chain from zero extension to an extension x_b is given by the integral over the force F_{wlc}

$$V_{wlc}(x) = \int_0^{x_b(i)} F_{wlc}(x') dx'. \quad (38)$$

In non-dimensional units the energy is

$$v_{wlc}(\xi_b(i)) = \frac{1}{\Lambda_p} \left\{ \frac{1}{4(1 - \xi_b(i))} + \frac{\xi_b^2(i)}{2} - \frac{\xi_b(i)}{4} - \frac{1}{4} \right\} \quad (39)$$

where the dimensionless persistence length is $\Lambda_p = L_p/L$. With the Boltzmann factor $e^{-v_{wlc}(\xi_b)}$ the density of unbound ligands at the transducer is

$$\rho(\xi_b(i)) = e^{-v_{wlc}(\xi_b(i)))}/Z(\xi_b(i)) \quad (40)$$

where

$$Z(\xi_b(i)) = \int_0^1 e^{-v(\xi)} d\xi + \int_0^{\xi_b(i)} e^{-v_{wlc}(\xi)} d\xi \quad (41)$$

is used as the partition sum. The first term is added to prevent the density from diverging at $\xi_b = 0$; for $v(\xi)$ a harmonic potential with the same force constant as for the worm-like chain was used. It takes into account that for entropic reasons the ligands are found on average at a certain height above the substrate. The exact distribution of the polymers in the presence of a wall is unknown [40]. In [15], it has been calculated by Monte Carlo simulations for a bead-pearl model. It was found that at large extensions, the distribution resembled that of a freely jointed chain [33]. The exact form of the distribution should have no influence on the generic aspects we are interested in. The distribution below the rest length is used only for normalization but is irrelevant for binding.

The forward rate of the adhesion cluster as function of the number of closed bonds i is

$$g(i) = \gamma(N_t - i)\rho(i), \quad (42)$$

where $\gamma = (k_{on}/k_0)(\ell_{bind}/L)$ has been defined. Equations (37) and (42) together with the master equation (1) and the deterministic equation (2) define the dynamical system. The six dimensionless parameters for the worm-like chain model are defined in analogy to those for the harmonic model. In the following we use $\Lambda_p = 1$, $\gamma = 1$, $\kappa_{wlc} = 1.5$ and $\phi_{wlc} = 0.1$. The choices for κ_{wlc} and ϕ_{wlc} mean that the properties of the tethers at small extension are similar as above for the harmonic tethers.

7.3 Analysis of the worm-like chain

A steady state analysis of the mean field equation (2) with the transition rates equations (37) and (42) from the worm-like chain model shows that the bifurcation behaviour is very similar to the one obtained for the linear
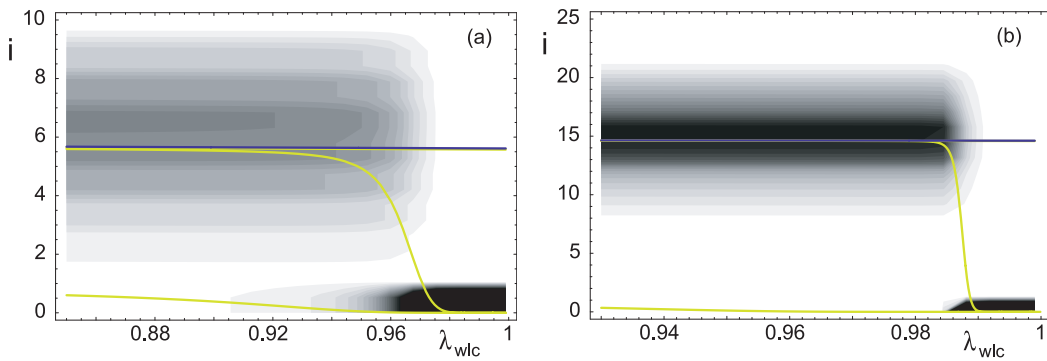
Fig. 10. Stationary probability distribution $\{p_i(\infty)\}_{i=0}^{N_t}$ from equation (28) with the transition rates equations (37) and (42) for the worm-like chain model and for cluster sizes (a) $N_t = 10$ and (b) $N_t = 25$ plotted as a function of the relaxed receptor-ligand distance λ_{wlc}. The other parameters are $\kappa_{wlc} = 1.5$, $\phi_{wlc} = 0.1$, $\Lambda_p = 1$ and $\gamma = 1$. The curves show the upper stable fixed point of the mean field equation, the average number of closed bonds in the bound and the unbound macrostate, and in the whole cluster, respectively.

springs, except that distances larger than $\lambda_{wlc} = 1$ are not possible due to the finite contour length. Figure 10 shows a density plot of the stationary probability distribution equation (28) for the worm-like chain transition rates equations (37) and (42) as function of λ_{wlc}. Together with the distribution, the dependence of the upper stable fixed point of the mean field equation and the average number of closed bonds of the full distribution as well as that of the bound and unbound macro-states are displayed. Again the binding region is bounded by the maximum extension $\lambda_{wlc} = \ell/L = 1$. As for the harmonic tethers a bimodal region is found in which two macrostates coexist. The average number of closed bonds in the bound state and the position of the maximum agree well with the upper stable fixed point of the deterministic equation. Both depend hardly on the receptor-ligand distance λ_{wlc}. The average number of closed bonds jumps from bound to unbound state in a discontinuous transition. This transition becomes sharper for larger clusters, that is, the width of the region in which both states are occupied to an appreciable degree decreases with increasing cluster size.

The physical reason for the striking plateau in the bound state is the non-linearity of the worm-like chain force extension relation, which reflects the strain-stiffening typical for biopolymers. A binding tether thus pulls the relatively soft transducer until the stiffnesses match, that is to the regime of harmonic tethers with $\kappa_{wlc} = 1.5$. Therefore, the final extension of the bound tethers decreases less than linear with λ_{wlc} and the effect on the number of closed bonds is weaker than for the harmonic model. If the transducer was replaced by another worm-like chain, the behavior of the system should be more like the harmonic model.

8 Conclusion

In this paper, we have introduced a stochastic model which allows to study the interplay of cooperative binding and unbinding for finite-sized adhesion clusters mediated by tethered ligands. Our model is based on established

principles of receptor-ligand binding, including Kramers-type rupture rates and separation-dependent binding rates based on the notion of an encounter complex. By implementing these principles in the framework of a one-step master equation, we were able to apply many powerful techniques from stochastic dynamics, including a Kramers-Moyal derivation of a Fokker-Planck equation (which in turn corresponds to a stochastic potential) and exact solutions for stationary solutions and mean first passage times. In particular, a bifurcation analysis based on the stochastic potential could be compared to the bifurcation analysis of the mean field equation to the master equation.

Our model shows that the simple mechanical model of Figure 1 can lead to a bistable situation in which two different states of adhesion, bound and unbound, coexist. The underlying reason for the occurrence of bistability is the existence of two mechanisms for positive feedback, one for rupture and one for binding. Cooperative bonds share the force exerted by the transducer so that the force exerted on each closed bond reduces upon binding. At the same time, the extension of the tethers reduces upon binding, which then increases the probability for further binding. In consequence, the transition rates in the master equation are both strongly non-linear functions of the number of closed bonds, which both can lead to positive feedback. This leads to an instability for the intermediate numbers of closed bonds and thus to bistability. The model discussed in this paper is an extension to a previously introduced model in which only the rupture rate was a non-linear function of the number of closed bonds [11, 21]. It could be re-obtained from the current model in the limit of a soft transducer, that is for $\kappa \to \infty$. In the present discussion, non-linear effects were mainly due to cooperative rebinding while the non-linearity of the rupture rate was weak.

In the mean field description, bistability leads to hysteresis for the binding and unbinding range: binding from the unbound state takes place at a smaller distance than unbinding from the bound state. Unlike for previous

discussions for non-cooperative bonds [16,17], this is not due to kinetic effects. In the stochastic description, the bistable system is characterized by a bimodal stationary probability distribution. Fluctuations over the barrier separating the stable states allow equilibration of the distribution. The time scale for equilibration has been calculated as the mean first passage time between the different adhesion states. Due to these finite transition times kinetic effects from changes of external parameters are important for the behavior of the system. In analogy to thermodynamic systems at first order phase transitions, changes of parameters on time scales smaller than the transition times allow occupation of the metastable states, while for slower changes, a stationary distribution will occur. In the bimodal region, the system frequently alternates between bound and unbound state. For large systems, the transition times become very large and the transition between bound and unbound becomes very sharp. The bimodal region in which two states are occupied to an appreciable and comparable amount becomes very small.

The predictions of this paper for the internal dynamics of adhesion clusters can be investigated with experimental setups like AFM or the surface force apparatus which allow to study the specific binding of two opposing surfaces with controlled separation. However, to map out the occupancy distribution for bound and unbound states could be tedious because of large transition times and low occupancy outside the dominant state. If measuring the binding range by stepwise reduction of the receptor-ligand distance, binding will take place when the transition time is smaller or equal to the waiting time. For large systems this will lead to hysteresis as in the deterministic case. For smaller systems, hysteresis will decrease due to the smaller transition times. In experiments with the surface forces apparatus [14,15], a behavior similar to the one predicted here has been observed. After initial binding a large attractive force was measured until an equilibrium position of the surfaces was established. In our model this increase would be due to the increased extension of the transducer spring. In those experiments, irreversible bonds with very large affinity have been used so that repeated transitions between bound and unbound states could not be observed.

In order to test our results, it would be necessary to use reversible adhesion bonds with low affinity. In general, binding through reversible bonds is highly relevant for biological systems. In particular, cell-matrix adhesion is mediated by reversible bonds like the ones between integrin-receptors in the plasma membrane and fibronectin in the extracellular environment. In this case, the equilibrium length of the ligand tether is $\ell_b = 11$ nm. Using the parameter values given in Table 1, one then finds from the stochastic model for $N_t = 5$ that for small adhesion clusters, bistability should occur around a relaxed receptor-ligand distance of 8 nm ($\lambda = 0.75$) [23]. Together with the ligand and receptor rest lengths, this results in a cell substrate distance of around 20 nm, that is the physiological value for cell-matrix adhesion [13]. Therefore the mechanism of bistability as described here can be used by cells to explore the extracellular space by many small and transient adhesions. On encountering favorable conditions, these small adhesions might mature, e.g. by recruitment of additional receptors. The results presented here show that this quickly leads to switching times which keep the adhesions in the bound macrostate.

In order to present a simple and reasonable model, here we have made the crucial assumption that all bonds are equivalent. This assumption leads to a one-step master equation and allows the application of many powerful tools from stochastic dynamics. In the future, our model could be extended to include additional aspects of biomimetic or biological systems, which usually however can not be described in the framework of a one-step master equation. In order to describe the growth and shrinkage of adhesion clusters, the overall number of bonds N_t should be made dynamic, possible involving regulation through the cytoskeleton. Assuming an elastic rather than a rigid transducer requires solution of elastic equations in order to derive the exact details of the force distribution. The force distribution would also be changed when accounting for possible curvature of the opposing surfaces. Finally it would also be interesting to consider the effect of disorder, e.g. in bond resting lengths or single bond on- and off-rates.

References

1. A. Bershadsky, B. Geiger, in *Guidebook to the extracellular matrix, anchor, and adhesion proteins*, edited by T. Kreis, R. Vale (Oxford University Press, Oxford, 1999), pp. 3–11
2. G.I. Bell, Science **200**, 618 (1978)
3. E. Evans, K. Ritchie, Biophys. J. **72**, 1541 (1997)
4. R. Merkel, P. Nassoy, A. Leung, K. Ritchie, E. Evans, Nature **397**, 50 (1999)
5. E. Evans, Annu. Rev. Biophys. Biomol. Struct. **30**, 105 (2001)
6. R. Merkel, Phys. Rep. **346**, 344 (2001)
7. M. Raible, M. Evstigneev, F.W. Bartels, R. Eckel, M. Nguyen-Duong, R. Merkel, R. Ros, D. Anselmetti, R. Reimann, Biophys. J. **90**, 3851 (2006)
8. E. Evans, K. Ritchie, Biophys. J. **76**, 2439 (1999)
9. U. Seifert, Phys. Rev. Lett. **84**, 2750 (2000)
10. U. Seifert, Europhys. Lett. **58**, 792 (2002)
11. T. Erdmann, U.S. Schwarz, Phys. Rev. Lett. **92**, 108102 (2004)
12. D. Leboeuf, N. Henry, Langmuir **22**, 127 (2006)
13. M. Cohen, D. Joester, B. Geiger, L. Addadi, Chem. Bio. Chem. **5**, 1393 (2004)
14. J.Y. Wong, T.L. Kuhl, J.N. Israelachvili, N. Mullah, S. Zalipsky, Science **275**, 820 (1997)
15. C. Jeppesen, J.Y. Wong, T.L. Kuhl, J.N. Israelachvili, N. Mullah, S. Zalipsky, C.M. Marques, Science **293**, 465 (2001)
16. A.G. Moreira, C. Jeppesen, F. Tanaka, C.M. Marques, Europhys. Lett. **62**, 876 (2003)

17. A.G. Moreira, C.M. Marques, J. Chem. Phys. **120**, 6229 (2004)
18. N.W. Moore, T.L. Kuhl, Biophys. J. **91**, 1675 (2006)
19. B. Geiger, A. Bershadsky, R. Pankov, K.M. Yamada, Nat. Rev. Mol. Cell Biol. **2**, 793 (2001)
20. P.W. Wiseman, C.M. Brown, D.J. Webb, B. Hebert, N.L. Johnson, J.A. Squier, M.H. Ellisman, A.F. Horwitz, J. Cell Sci. **117**, 5521 (2004)
21. T. Erdmann, U.S. Schwarz, J. Chem. Phys. **121**, 8997 (2004)
22. T. Erdmann, U.S. Schwarz, Europhys. Lett. **66**, 603 (2004)
23. T. Erdmann, U.S. Schwarz, Biophys. J. **91**, L60 (2006)
24. N.G. van Kampen, *Stochastic Processes in Physics and Chemistry* (Elsevier, Amsterdam, 2003)
25. H. Risken, *The Fokker-Planck Equation* (Springer-Verlag, Heidelberg, 1989)
26. P. Hanggi, H. Grabert, P. Talkner, H. Thomas, Phys. Rev. A **29**, 371 (1984)
27. M. Eigen, in *Quantum statistical mechanics in the natural sciences*, edited by S.L. Minz, S.M. Wiedermayer (Plenum, New York, 1974), pp. 37–61

28. H.C. Berg, E.M. Purcell, Biophys. J. **20**, 193 (1977)
29. D. Shoup, A. Szabo, Biophys. J. **40**, 33 (1982)
30. G. Schreiber, Curr. Opin. Struct. Biol. **12**, 41 (2002)
31. M. Nguyen-Duong, K.W. Koch, R. Merkel, Europhys. Lett. **61**, 845 (2003)
32. R. Merkel, Physics Reports **346**, 343 (2001)
33. M. Doi, S.F. Edwards, *The theory of polymer dynamics* (Clarendon, Oxford, 1986)
34. J.J. Tyson, K.C. Chen, B. Novak, Current Opinion in Cell Biology **15**, 221 (2003)
35. W. Horsthemke, R. Lefever, *Noise-induced transitions* (Springer, Berlin, 1984)
36. D.T. Gillespie, J. Comp. Phys. **22**, 403 (1976)
37. D.T. Gillespie, J. Phys. Chem. **81**, 2340 (1977)
38. J.F. Marko, E.D. Siggia, *Macromolecules* **28**, 8759 (1995)
39. J. Kierfeld, O. Niamploy, V. Sa-yakanit, R. Lipowsky, Euro. Phys. J. E **14**, 17 (2004)
40. M. Koch, J.-U. Sommer, A. Blumen, J. Chem. Phys. **106**, 1248 (1996)